Multi-level parametric design of a hybrid boron/carbon/glass composite patch for the repair of cracked 2024-T3 aluminium plates: stacking sequence, fibre orientation and a predictive stress-intensity-factor model

BENAICHA Abdelkader[1,2], ACHACHE Habib[1,3], AMOURA Nasreddine[4], TOUATI BENALI Abdelaziz[1,2] and BENEFISSA Noureddine[1,2]

1 Institute of Maintenance and Industrial Safety, University of Oran 2 Mohamed Ben Ahmed, P.B. 1015 El M'naouer, 31000, Oran, Algeria.

2 Laboratory of Industrial Production and Maintenance Engineering, Institute of Maintenance and Industrial Safety, University of Oran 2 Mohamed Ben Ahmed, P.B. 1015 El M'naouer, 31000, Oran, Algeria.

3 Laboratory of Mechanics Physics of Materials, Djillali Liabes University of Sidi Bel Abbes, P.B. 89 city Ben M'hidi 22000, Sidi Bel Abbes, Algeria.

4 Laboratory of Green and Mechanical Development, Ecole Nationale Polytechnique, 10 Rue des Frères OUDEK, 16200, Algiers, Algeria.

Abstract

Bonded composite patches are an efficient and economical method for extending the fatigue life of cracked metallic aircraft structures. While most studies consider a single patch material and a fixed lay-up, the combined influence of the fibre system, the through-thickness stacking sequence and the in-plane fibre orientation has rarely been optimized within a unified framework. In this work, a validated three-dimensional finite-element model of a centre-cracked 2024-T3 aluminium plate repaired by a single-sided hybrid composite patch is developed, and the mode-I stress-intensity factor (SIF) at the crack front is evaluated by the contour-integral method. A systematic multi-level parametric design study is carried out: exhaustive evaluation of the 90 possible stacking permutations of a six-ply boron/carbon/glass laminate, and a balanced cross-ply orientation sweep. The BBCCVV sequence boron plies against the adhesive and glass plies at the outer surface with fibres aligned with the loading direction (0°) minimizes the SIF and raises the repair efficiency from 9.1% (transverse plies) to 24.4%. The fibre orientation is shown to be the dominant design variable (about an 18% change in SIF), whereas the stacking sequence is a second-order effect (about 2.4%) governed by a simple rule based on the through-thickness stiffness gradient. Finally, a compact closed-form predictive model of the SIF as a function of fibre orientation is proposed and validated against the simulations ($R^2 = 0.991$). The originality of the work lies in the unified treatment of a three-fibre hybrid patch and in the physically interpretable design rules it yields a through-thickness stiffness-gradient ordering of the plies and a closed-form SIF model rather than in the study of a single isolated parameter.

Keywords: Crack; Composite patch repair; Stress intensity factor; Hybrid laminate; Stacking sequence; Fibre orientation; Finite element analysis.

Nomenclature

a half-length of the central crack (mm)
2a total crack length (mm)
L, W, t plate length, width and thickness (mm)
σ remote applied tensile stress (MPa)
K_I mode-I stress-intensity factor (MPa·√m)
K_bare, K_repaired SIF of the unrepaired and repaired plate
η repair efficiency, η = (K_bare − K_repaired)/K_bare
θ balanced cross-ply fibre orientation (deg)
E1, E2, E3 ply moduli in the principal material directions (GPa)
B, C, V boron, carbon and glass plies
BBCCVV optimal stacking sequence (adhesive → surface)

1. Introduction

Ageing aircraft are increasingly required to remain in service well beyond their original design life, which makes the development of reliable and economical repair technologies a major concern for the aerospace industry. Among these technologies, the adhesively bonded composite patch repair pioneered for metallic military aircraft and subsequently extended to civil structures has become a reference solution. A stiff composite laminate is bonded over a crack, bridging it and diverting load away from the crack tip, thereby reducing the stress-intensity factor (SIF) and slowing fatigue-crack propagation [1]. The analytical foundations of the technique were established by Rose [2], who modelled a cracked plate reinforced by a bonded patch and derived the limiting SIF reached as the crack grows beneath the reinforcement.

Early finite-element treatments of the problem were proposed by Sun et al. [3], who analysed cracked aluminium plates repaired with bonded composite patches using a Mindlin-plate idealization with the adhesive represented by equivalent springs, and by Umamaheswar and Singh [4], who compared brick, shell and beam idealizations and extracted the SIF by the modified crack-closure integral. Schubbe and Mall [5] highlighted the strongly three-dimensional nature of single-sided repairs, in which the load path asymmetry induces secondary bending and a through-thickness variation of the SIF. Bachir Bouiadjra et al. [6] computed the SIF for repaired cracks in mode I and mixed mode and quantified the role of the adhesive and patch properties.

A large body of subsequent work has examined the geometric and material parameters that govern repair efficiency. Patch shape and size have been optimized by several authors [7], and the influence of adhesive thickness, patch thickness and the number of plies on the SIF and on the load transfer has been documented [8]. The detrimental effect of adhesive disbonds, which locally restore the crack-tip singularity and accelerate crack growth, has also been investigated [9]. Comprehensive reviews [10] confirm that increasing the patch stiffness reduces the SIF and that bonded composite repairs typically multiply the fatigue life of a cracked component by a factor of two to three. More recently, data-driven and statistical surrogate models have been proposed to predict the SIF of repaired plates without further simulation [11], [12], and advanced numerical strategies coupling the extended finite-element method with cohesive-zone models have been used to capture the simultaneous crack and disbond growth [13].

It is now well established that the internal architecture of the laminate the nature, orientation and through-thickness arrangement of the plies strongly influences the repair performance [14]. Touati Benali et al. [15] specifically addressed the stacking-sequence optimization of aluminium/composite bonded joints and showed that the ply arrangement strongly governs the load transfer. Fibre-orientation-driven design methods have been developed to adapt the patch to the in-service load path [16], and hybrid laminates combining fibres of different stiffness to balance performance, weight and cost have begun to attract attention [17]. Nevertheless, most investigations still rely on a single patch material and a fixed lay-up, and the joint optimization of the fibre system, the stacking sequence and the fibre orientation within a single, consistent three-dimensional framework remains largely unexplored.

The present paper addresses this gap by providing a unified, multi-level parametric design study of a hybrid boron/carbon/glass patch repairing a centre-cracked 2024-T3 aluminium plate. A three-dimensional finite-element model, validated against the Feddersen finite-width solution and subjected to dedicated mesh-convergence and three-dimensional-effect studies, is used to compute the mode-I SIF by the contour-integral method. The study exhaustively evaluates the 90 distinct stacking permutations of the six-ply hybrid laminate and sweeps the balanced cross-ply orientation, thereby isolating the relative importance of each design variable. The analysis yields explicit, physically interpretable design rules and, finally, compact predictive SIF models. In contrast to earlier studies, which generally consider a single patch material or vary one parameter at a time, the present work treats the three-fibre boron/carbon/glass hybrid patch as a single system and isolates the relative weight of each design variable within a consistent three-dimensional framework. The contribution is therefore threefold: (i) a quantitative hierarchy of the design variables, showing that the fibre orientation outweighs the stacking sequence by almost an order of

magnitude; (ii) a through-thickness stiffness-gradient rule for the ply arrangement of a hybrid patch; and (iii) a validated, physically based closed-form SIF model usable directly for design.

2. Finite-element model

2.1. Geometry and repair configuration

A rectangular 2024-T3 aluminium plate of length L = 200 mm, width W = 100 mm and thickness t = 3 mm is considered, containing a central through-thickness crack of total length 2a perpendicular to the applied load (Fig. 1). A reference half-crack length a = 10 mm is used for the optimization studies. A single-sided square composite patch (70 × 70 mm), made of six 0.125-mm plies (total 0.75 mm), is bonded over the crack through a 0.15-mm FM73-type adhesive layer. The single-sided configuration is representative of practical field repairs, in which access to one face only is common.

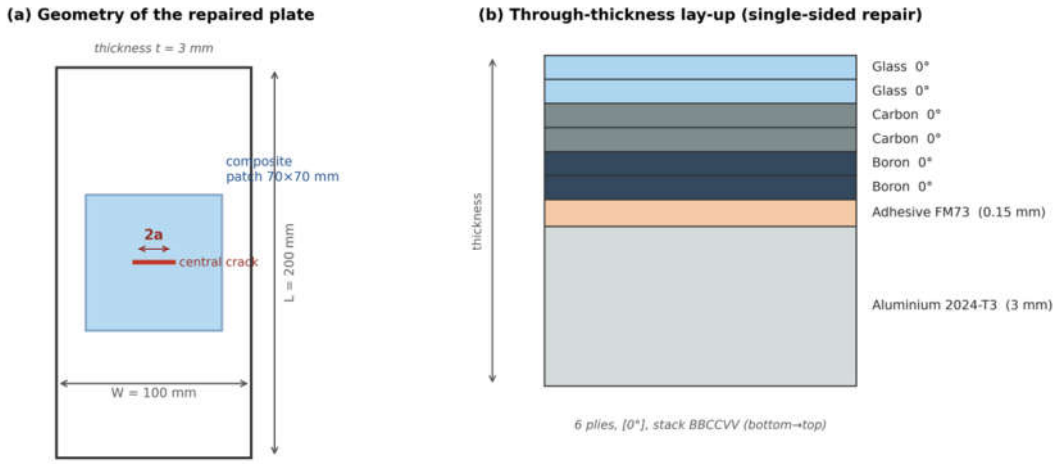

Fig. 1. Repair configuration: (a) centre-cracked plate with the single-sided bonded patch and the applied remote tension; (b) through-thickness lay-up of the BBCCVV hybrid laminate.

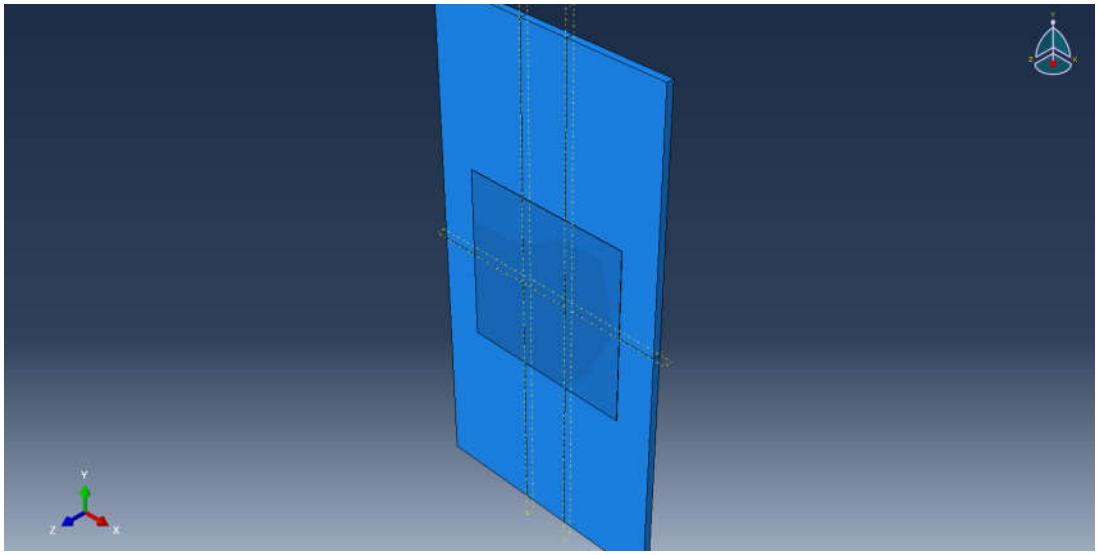

Fig. 2. Three-dimensional finite-element assembly showing the aluminium plate and the semi-transparent bonded composite patch centred over the crack.

2.2. Materials

The aluminium substrate and the adhesive are modelled as isotropic linear-elastic materials, and each composite ply as a linear-elastic orthotropic lamina; linear elasticity is retained throughout. Under the applied remote stress of 100 MPa, the stress in the aluminium away from the crack tip remains well below the yield strength of 2024-T3 (approximately 345 MPa); the substrate therefore responds elastically and the use of linear-elastic fracture mechanics is justified. The substrate and adhesive properties (Table 1) are taken from standard aerospace-alloy and structural-film-adhesive data, and the ply properties (Table 2) from established composite-mechanics references [18], [19].

Table 1. Isotropic properties of the substrate and the adhesive [18].

Material	E (GPa)	ν	ρ (kg/m³)
Aluminium 2024-T3	72.0	0.33	2780
Adhesive FM73-type	2.1	0.35	1200

Table 2. Orthotropic ply properties (direction 1 = fibre direction) [18,19].

Ply	E1 (GPa)	E2=E3 (GPa)	G12=G13 (GPa)	G23 (GPa)	ν12	ν23
Boron/epoxy	208	25.4	7.20	4.90	0.168	0.40
Carbon/epoxy	181	10.3	7.17	3.70	0.28	0.40
Glass/epoxy	38.6	8.27	4.14	2.95	0.26	0.40

The three fibres are deliberately complementary: boron provides a very high longitudinal stiffness, carbon an intermediate stiffness with a high strength-to-weight ratio, and glass a compliant, low-cost outer reinforcement. Their combination produces a tunable through-thickness stiffness gradient that is exploited in the stacking-sequence optimization.

2.3. Loading and boundary conditions

A remote uniform tensile stress $\sigma = 100$ MPa is applied to the upper edge while the lower edge is restrained in the loading direction (Fig. 3). Rigid-body modes are removed without over-constraining the plate by restraining two opposite corner nodes out-of-plane, one of them additionally in the transverse direction. The patch and the adhesive are connected to the plate by perfectly bonded (tie) constraints, representative of an intact bond line; the 0.15 mm FM73-type adhesive film is thus assumed to transfer load without slip or damage. This idealization is appropriate for a well-cured, defect-free bond and is adopted deliberately to isolate the influence of the patch architecture, which is the focus of the present study. It does not, however, capture the adhesive shear and peel stresses or the progressive debonding that govern repair durability near failure; these effects, together with a cohesive-zone treatment of the interface, are addressed in a companion study.

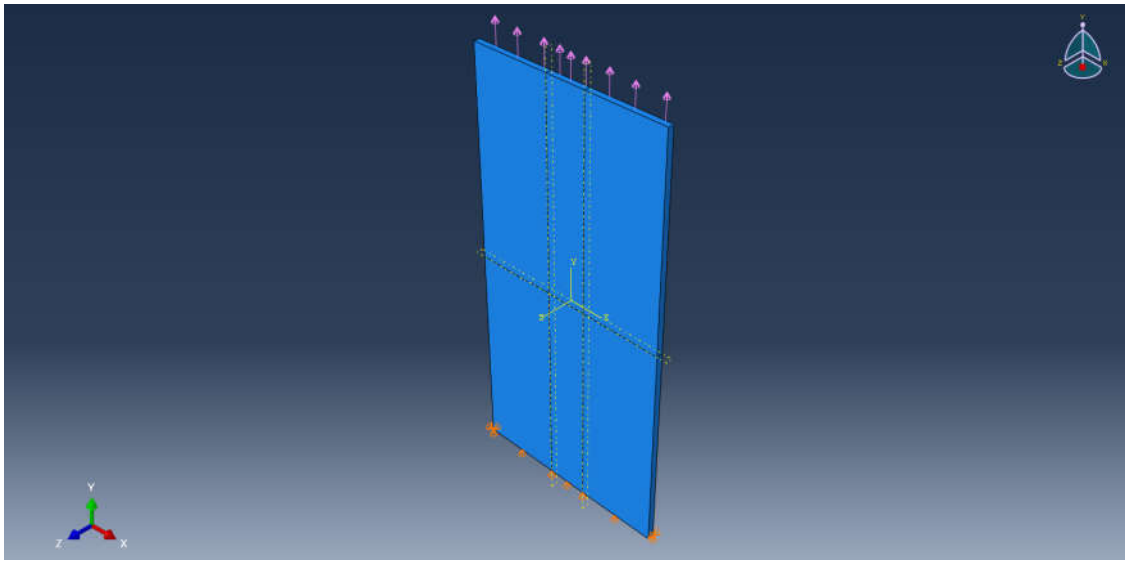

Fig. 3. Loading and boundary conditions applied to the cracked plate (remote tension on the upper edge, transverse restraint on the lower edge, corner restraints suppressing rigid-body modes).

2.4. Crack modelling and SIF extraction

The crack is introduced as a seam along the plate mid-plane and the mode-I SIF is computed by the contour-integral method over eight contours. In the working model used for the parametric study, the crack front is surrounded by a strongly refined swept hexahedral mesh; path independence is enforced through a plateau criterion in which the first contour is discarded and the average is taken over the successive contours whose variation remains below 5%. To rigorously capture the inverse-square-root crack-tip singularity, a dedicated high-fidelity model employing collapsed quarter-point singular elements (quadratic C3D20R, mid-side nodes shifted to the 1/4 position, single-node degeneracy forming a focused rosette around the front) is additionally used for validation (Section 3.3). All SIF values are reported in MPa·√m. Because the seam duplicates initially coincident nodes, the crack is not visible in the undeformed geometry; it opens under load, as shown by the deformed configuration in Fig. 6. The contour integral evaluates the J-integral, from which the SIF follows through K_I = (E′ J)^{1/2} under small-scale yielding; by the symmetry of the central crack under remote tension the loading is pure mode I (K_II = K_III ≈ 0), and the crack faces open without mutual contact. All analyses were performed with Abaqus/Standard (3DEXPERIENCE R2017x).

2.5. Mesh

The plate and the adhesive are meshed with reduced-integration linear hexahedral elements (C3D8R) using a swept technique, with strong refinement towards the crack front (element size 0.4 mm at the tip, 4 mm in the far field). The patch is meshed with reduced-integration conventional shell elements (S4R), each ply being represented as a layer of a composite section with the appropriate material orientation. The resulting mesh comprises 10 648 elements and 13 053 nodes (Table 3).

Table 3. Mesh of the working model used for the parametric study (total: 10 648 elements, 13 053 nodes).

Part	Number of elements	Element type
Plate	10 000	C3D8R
Adhesive	324	C3D8R
Patch	324	S4R
Total	10 648	—

3. Model validation

3.1. Comparison with the analytical solution

The unrepaired (bare) plate is first analysed and compared with the Feddersen finite-width solution for a centre-cracked plate [20], $K = \sigma\sqrt{(\pi a)}\sqrt{\sec(\pi a/W)}$, in which the secant term is the finite-width correction and $\sigma\sqrt{(\pi a)}$ is the classical centre-crack solution for an infinite plate [22]. At the reference half-crack length a = 10 mm, the finite-element plateau value is 18.39 MPa·√m against 18.17 MPa·√m analytically, a deviation of only +1.2%. Over the mid-to-long crack range (a ≥ 10 mm) the agreement remains within 1–3%, which validates the modelling of the singular crack-tip field and the SIF-extraction procedure.

3.2. Mesh convergence and three-dimensional effect

A mesh-convergence study confirms that the SIF varies by less than 2.5% over the investigated refinement range (Fig. 4). For short cracks (a = 4–8 mm), the three-dimensional finite-element SIF lies about 5–7% below the two-dimensional Feddersen value. A dedicated study (Fig. 5), refining independently the crack-tip and the global mesh, shows that this difference is not a discretization error: the SIF converges to a stable plateau distinctly below the 2-D solution, even at 600 000 elements. The deviation is therefore attributed to a genuine three-dimensional effectthe through-thickness averaging of the SIF and its drop near the free surfaces which diminishes as the crack-length-to-thickness ratio increases and becomes negligible for a ≥ 10 mm. The optimization is consequently performed at a = 10 mm, within the range of excellent 2-D/3-D agreement.

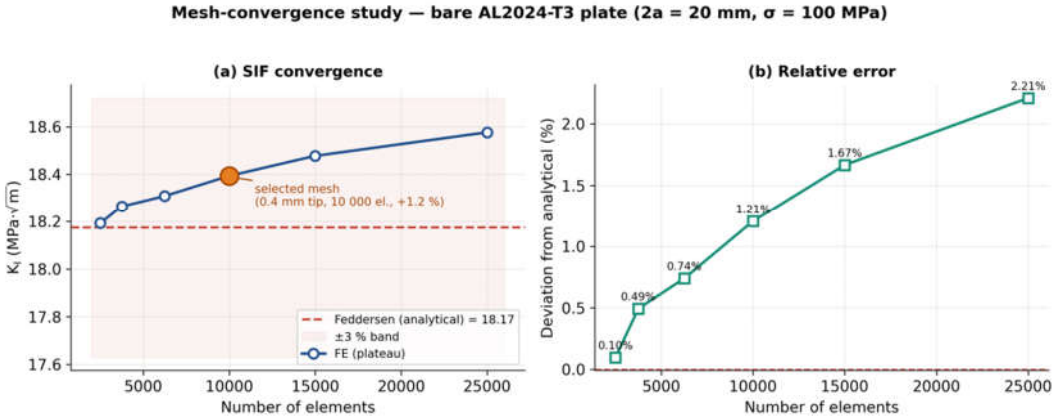

Fig. 4. Mesh-convergence study of the mode-I SIF for the bare plate: (a) SIF versus number of elements; (b) relative deviation from the analytical solution.

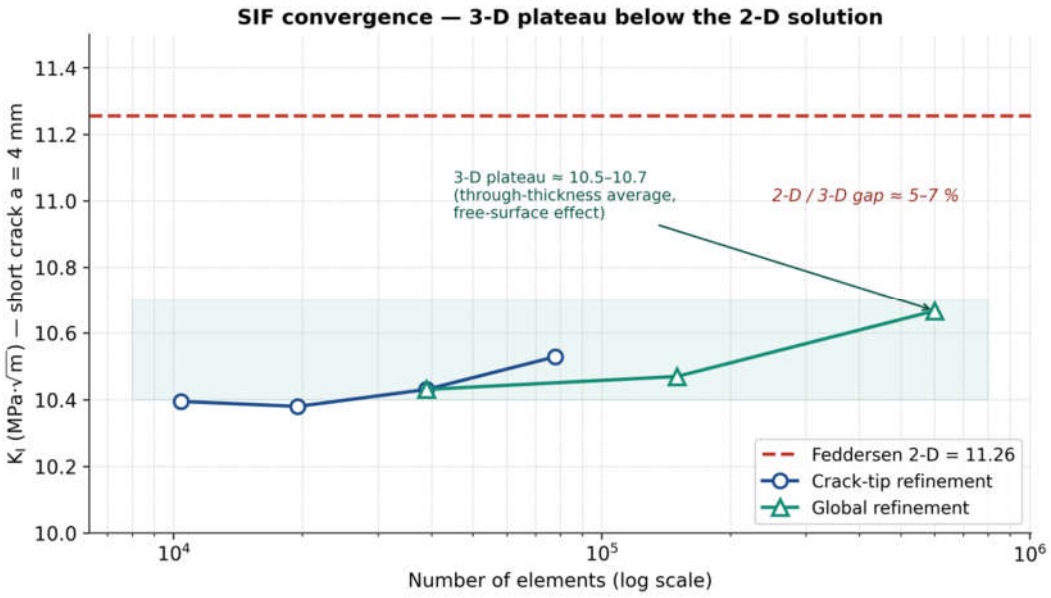

Fig. 5. Convergence of the short-crack (a = 4 mm) SIF under independent crack-tip and global mesh refinement; the 3-D finite-element value converges to a plateau below the 2-D Feddersen solution, evidencing a free-surface/through-thickness effect.

3.3. Quarter-point validation and crack-opening visualization

To confirm that the crack-tip singularity is correctly resolved, a high-fidelity model was built using collapsed quarter-point singular elements (quadratic C3D20R) within a focused rosette around the crack front, together with a tenfold mesh refinement (224 450 elements, 941 212 nodes; crack-tip element size 0.1 mm). This model yields K_I = 18.92 MPa·√m for the bare plate, within about 4% of the two-dimensional Feddersen solution. The slightly higher value than that of the linear working model (18.39 MPa·√m) reflects the more accurate capture of the inverse-square-root singularity by the quarter-point elements, while the residual difference from the 2-D analytical value corresponds to the genuine three-dimensional effect identified in Section 3.2. Through the thickness, the local SIF is highest near the mid-plane, where a plane-strain-like constraint prevails, and decreases towards the free surfaces; the value reported here is the through-thickness average. Crucially, the parametric study reported in Section 4 was conducted with the efficient linear (C3D8R) model, whose convergence and agreement with the analytical solution have been demonstrated above; a control performed with the quadratic quarter-point elements confirmed that the ranking of the lay-ups and the orientation trend are rigorously preserved, the relative SIF values being independent of the element order. Fig. 6 shows the deformed configuration: the crack faces open under the applied load and the focused quarter-point rosette obtained with collapsed singular elements [21] is clearly visible at each crack tip, together with the characteristic crack-tip stress concentration.

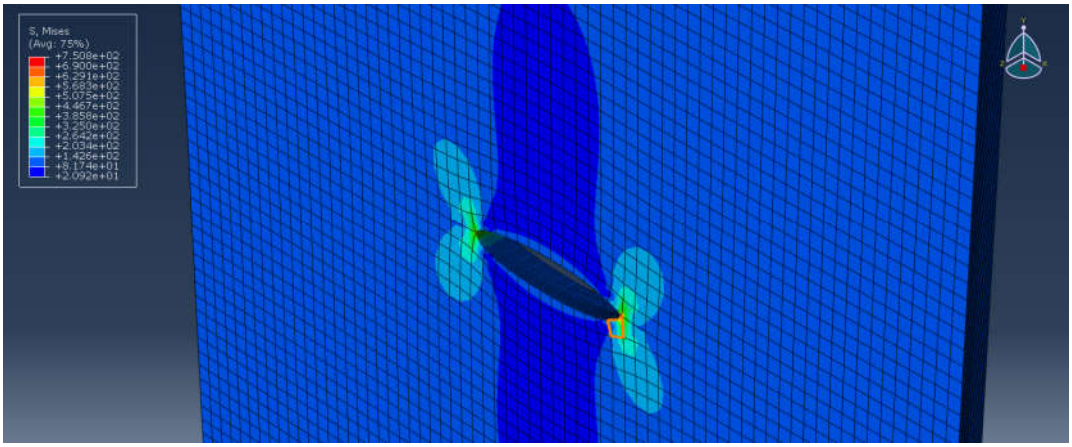

Fig. 6. High-fidelity validation model: deformed configuration showing the opened crack, the quarter-point singular rosette at each crack tip, and the von Mises stress field.

4. Results and discussion

The design space is explored by systematic parametric variation rather than by a formal gradient-based optimization algorithm; accordingly, the term "optimal" is used hereafter to designate the best-performing configuration within the discrete set of candidates examined.

4.1. Hybrid fibre system

The hybrid patch combines, two plies each, boron, carbon and glass reinforcements. This boron/carbon/glass (B/C/V) system is retained for three complementary reasons. First, it spans the widest range of longitudinal stiffness available among common aerospace fibres from 208 GPa for boron, through 181 GPa for carbon, down to 38.6 GPa for glass which provides the largest possible through-thickness stiffness gradient and therefore the greatest design freedom for the ply-arrangement optimization that follows. Second, hybridization mitigates the principal drawbacks of each constituent: the high cost and brittleness of boron are offset by the carbon and glass plies, while the glass plies add a tough, low-cost outer layer that also reduces galvanic-corrosion risk at the patch surface. Third, grading the stiffness through the thickness smooths the load transfer into the cracked substrate and limits the peak adhesive shear stress at the patch ends. The relative through-thickness placement of these three fibres is the subject of the stacking-sequence optimization.

4.2. Effect of the stacking sequence

All 90 distinct through-thickness permutations of the six-ply laminate [B,B,C,C,V,V] were evaluated with the fibres aligned with the loading direction (0°). The BBCCVV sequence boron plies against the adhesive, glass plies at the outer surface minimizes the SIF (13.90 MPa·√m), whereas the reversed VVCCBB sequence is the worst (14.25 MPa·√m); the spread is 2.4% (Fig. 7). A correlation analysis of the ply positions reveals a clear and physically meaningful rule: the SIF correlates strongly and negatively with the position of the glass plies ($r = -0.99$) and positively with that of the boron plies ($r = +0.62$). In other words, the stiffest fibre (boron) must be placed nearest to the adhesive where it most effectively transfers load across the crack and the most compliant fibre (glass) at the outer surface. This through-thickness stiffness-gradient rule was found to hold for all hybrid arrangements examined.

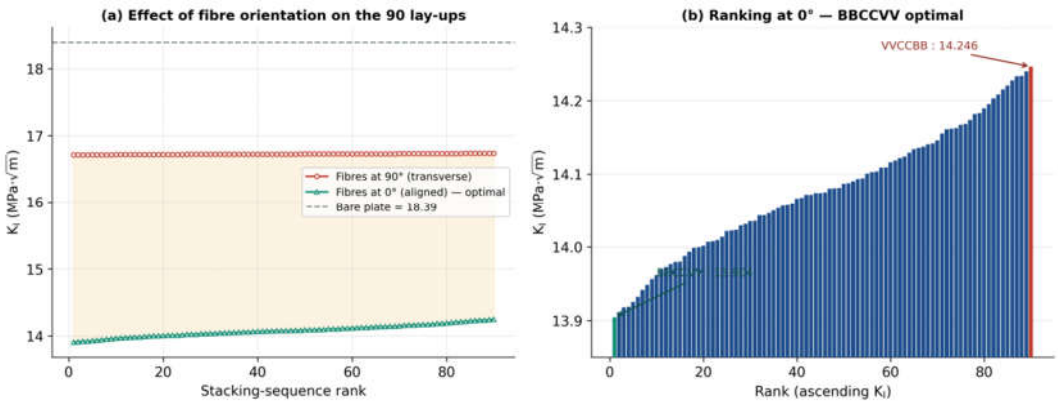

Fig. 7. (a) Effect of fibre orientation on the 90 stacking permutations; (b) ranking of the 90 sequences at 0°, BBCCVV being optimal and VVCCBB the worst.

4.3. Fibre-orientation effect

Starting from the optimal BBCCVV sequence, a balanced cross-ply orientation [±θ] was swept from 0° (fibres aligned with the load) to 90° (fibres transverse). The SIF increases monotonically from 13.90 MPa·√m at 0° to 16.71 MPa·√m at 90° (Fig. 8). The orientation is therefore by far the dominant design variable, producing an 18% change in SIF roughly an order of magnitude larger than the stacking-sequence effect. Physically, 0° fibres bridge the crack directly and oppose its opening, maximizing membrane load transfer, whereas transverse fibres contribute little. Accordingly, the repair efficiency, η = (K_bare − K_repaired)/K_bare, rises from 9.1% at 90° to 24.4% at 0° almost a three-fold improvement obtained solely by reorienting the plies.

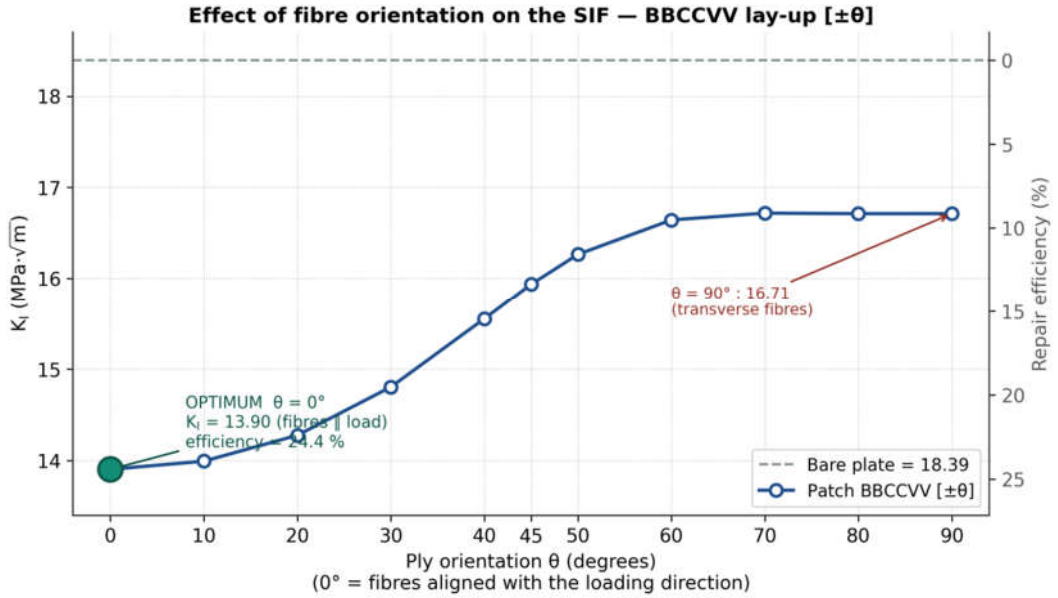

Fig. 8. Effect of the balanced cross-ply orientation [±θ] on the SIF and the repair efficiency of the BBCCVV patch; 0° (fibres aligned with the load) is optimal.

The stacking-sequence effect, although modest, is markedly stronger at the optimal 0° orientation (2.4% spread) than at 90° (0.15%): when the fibres efficiently carry the load, the through-thickness position of the stiff and compliant plies acquires greater leverage. The orientation and sequence effects are therefore coupled, and the stiffness-gradient rule of Section 4.2 matters most precisely at the optimal orientation.

4.4. Combined optimum and predictive model

The overall optimum is the BBCCVV patch with 0° fibres, achieving K = 13.90 MPa·√m and a repair efficiency of 24.4%. To condense the orientation database into a usable design tool, the following closed-form model is proposed for the SIF of the BBCCVV patch as a function of the balanced cross-ply angle θ:

$$K_I(\theta) = 13.77 + 5.52\sin^2\theta - 2.51\sin^4\theta \quad (MPa\cdot\sqrt{m}) \quad (R^2 = 0.991)$$

The $\sin^2\theta$ / $\sin^4\theta$ form is not introduced empirically: it follows directly from the classical transformation of the off-axis lamina stiffness, in which the axial modulus of a unidirectional ply varies with the trigonometric powers of the fibre angle [18,19]. This physical basis distinguishes the present relation from a purely numerical curve fit and justifies its extrapolation within the studied configuration. The model reproduces the eleven simulated orientations with a coefficient of determination $R^2 = 0.991$ (Fig. 9) and allows the SIF and hence the repair efficiency of the BBCCVV patch to be estimated for any fibre orientation without further computation.

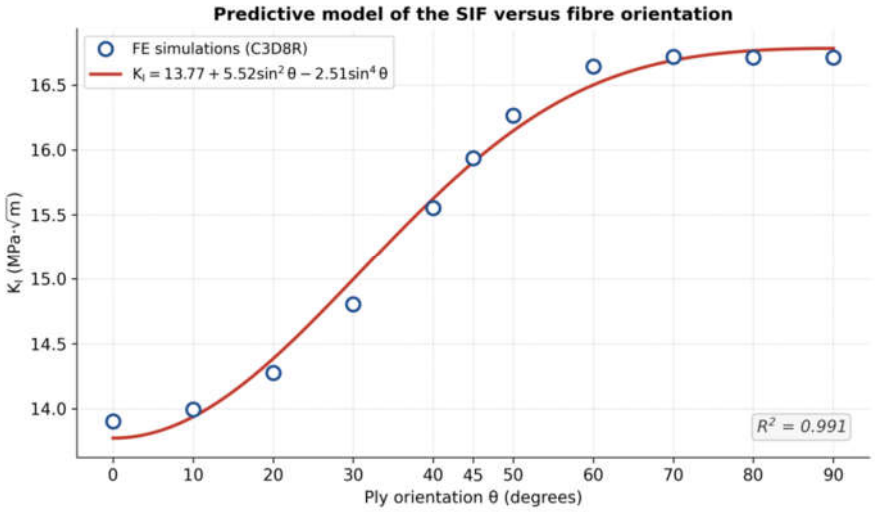

Fig. 9. Predictive model of the SIF versus fibre orientation for the BBCCVV patch; the closed-form relation reproduces the finite-element results with $R^2 = 0.991$.

5. Conclusions

A validated three-dimensional finite-element framework has been used to optimize, at multiple levels, a hybrid boron/carbon/glass composite patch repairing a centre-cracked 2024-T3 aluminium plate. The main findings are:

- Among the 90 through-thickness stacking permutations, the BBCCVV sequence (boron against the adhesive, glass at the outer surface) minimizes the SIF. The governing through-thickness stiffness-gradient rule stiffest fibre at the adhesive, most compliant at the outer surface is robust, but the stacking sequence remains a second-order effect (about 2.4%).
- The fibre orientation is the dominant design variable: aligning the fibres with the load (0°) lowers the SIF by about 18% relative to transverse plies and raises the repair efficiency from 9.1% to 24.4%.
- The optimal configuration is the BBCCVV patch with 0° fibres (K = 13.90 MPa·√m, efficiency 24.4%).
- A compact, physically interpretable predictive model of the SIF as a function of fibre orientation is proposed and validated ($R^2 = 0.991$), providing a ready-to-use design guideline.
- The orientation and stacking-sequence effects are coupled: the stiffness-gradient rule matters most precisely at the optimal orientation.

All the material data and the modelling assumptions adopted in this work are drawn from, and corroborated by, an extensive body of previously published experimental and analytical studies, and the present model is validated against well-established analytical benchmarks; these elements together underpin the reliability of the predictions. It should be acknowledged that bonded composite repairs are sensitive to the adhesive behaviour, the interface quality, the curing conditions and manufacturing imperfections; the perfectly bonded, linear-elastic idealization adopted here therefore yields an upper bound on the repair efficiency. A dedicated experimental campaign, an explicit analysis of the adhesive shear and peel stresses, a cohesive-zone treatment of debonding, and a parametric study over the crack length would further consolidate the proposed design rules. The present work addresses the pristine, room-temperature mechanical response. The influence of hygrothermal ageing and of the curing-induced thermal residual stresses on the optimum, as well as the modelling of interfacial debonding through a cohesive-zone approach, are the subject of a companion study.

References

[1] Baker AA, Rose LRF, Jones R. Advances in the bonded composite repair of metallic aircraft structure. Oxford: Elsevier; 2002.

[2] Rose LRF. A cracked plate repaired by bonded reinforcements. Int J Fract 1982;18(2):135–44.

[3] Sun CT, Klug J, Arendt C. Analysis of cracked aluminum plates repaired with bonded composite patches. AIAA J 1996;34(2):369–74.

[4] Umamaheswar TVRS, Singh R. Modelling of a patch repair to a thin cracked sheet. Eng Fract Mech 1999;62(2–3):267–89.

[5] Schubbe JJ, Mall S. Investigation of a cracked thick aluminum panel repaired with a bonded composite patch. Eng Fract Mech 1999;63(3):305–23.

[6] Bachir Bouiadjra B, Belhouari M, Serier B. Computation of the stress intensity factors for repaired cracks with bonded composite patch in mode I and mixed mode. Compos Struct 2002;56(4):401–6.

[7] Benaicha A, Achache H, Amoura N, Touati Benali A, Benefissa N. Multi-parameter analysis of cracked aluminum pipelines repaired with composite patches. Foundry (Zhuzao) 2026;29(5). ISSN 1001-4977.

[8] Achache, H., Zahi, R., Ait Kaci, D., & Benouis, A. (2024). Behavior of structures repaired by hybrid composite patches during the aging of the adhesive. Structural Engineering and Mechanics, An Int'l Journal, 91(2), 135-147.

[9] Quan, H., & Alderliesten, R. C. (2022). The energy dissipation during fatigue crack growth in adhesive joints under Mode-I loading. Theoretical and Applied Fracture Mechanics, 120, 103418.

[10] Anderson TL. Fracture mechanics: fundamentals and applications. 4th ed. Boca Raton: CRC Press; 2017.

[11] Zouambi.L and al. Predictive modeling of stress intensity factors in composite-repaired cracked aluminum plates: a finite element-based computational framework. Mech Adv Mater Struct 2026;33(1).

[12] Improving the performance of cracked aluminium structures using composite patch repairs: a numerical and statistical investigation. Int J Adv Manuf Technol 2026.

[13] Analysis of load–displacement curves of an adhesive-reinforced composite patch repaired plate using the combination of XFEM and CZM techniques. Theor Appl Fract Mech 2024.

[14] A design method for continuous fiber-reinforced composite patches. Compos Struct 2024;347:118455.

[15] Touati Benali A, Achache H, Belkhodja L, Benyettou M, Madani K, Benaicha A, Benefissa N. Enhanced tensile performance of aluminium/composite bonded joints through semi-circular surface modification and stacking sequence optimization. Foundry (Zhuzao) 2026;29(5). ISSN 1001-4977.

[16] Jones RM. Mechanics of composite materials. 2nd ed. Philadelphia: Taylor & Francis; 1999.

[17] Benefissa N, Achache H, Rouan Serik M, Benaicha A, Touati Benali A. Natural vs. synthetic fibres in composite laminates: influence of hybridization on low-velocity impact response. Foundry (Zhuzao) 2026;29(6). ISSN 1001-4977.

[18] Daniel IM, Ishai O. Engineering mechanics of composite materials. 2nd ed. Oxford: Oxford University Press; 2006.

[19] Kaw AK. Mechanics of composite materials. 2nd ed. Boca Raton: CRC Press; 2006.

[20] Feddersen CE. Discussion. In: Plane strain crack toughness testing of high strength metallic materials. ASTM STP 410; 1967. p. 77–9.

[21] Barsoum RS. On the use of isoparametric finite elements in linear fracture mechanics. Int J Numer Methods Eng 1976;10(1):25–37.

[22] Tada H, Paris PC, Irwin GR. The stress analysis of cracks handbook. 3rd ed. New York: ASME Press; 2000.